ORIGINAL ARTICLE

Highly Accurate Brain Tumor Segmentation and Classification Using Multiple Feature Sets

Megha Sunil Borse[1*] (ID) , Murali Prasad R [2], Tummala Ranga Babu [3]

[1] *Department of Electronics and Telecommunication Engineering, Cummins College of Engineering for Women, Karvenagar, Pune, India*

[2] *Department of Electronics and Communication Engineering, Marri Laxman Reddy Institute of Technology and Management, Dundigal, Hyderabad, India*

[3] *Electronics & Communication Engineering, Rayapati Venkata Rangarao & Jagarlamudi Chandramouli College of Engineering, Guntur, India*

*Corresponding Author: Megha Sunil Borse
Email: megha.borse@cumminscollege.in

Abstract

Purpose: Nowadays, detecting brain tumors is a crucial application. If a tumor is discovered later on, the medical issues are significant. Therefore, early diagnosis is essential. Magnetic Resonance Imaging (MRI) is the most recent detection, diagnosis, and assessment technology.

Materials and Methods: In this study, MRI images are segmented before input to a pulse-coupled neural network model to identify the existence of a tumor in the brain picture. The doctor may turn to this model for assistance if there are more input MRI brain pictures. This work preprocesses the images using normalization smoothing with linear filter and adaptive histogram. Statistical and Local Binary Patterns (LBP) features are extracted from the preprocessed images to perform the classification process. The Deep Convolutional Network (DCNN) is used to segment the image. The Pulse Coupled Neural Networks (PCNN) categorize the input images as normal and tumor.

Results: Accuracy, sensitivity, specificity, and precision are the various metrics evaluated. This work achieves 99.35 accuracies, 99.78 sensitivity, 98.45 specificities, and 97.61 precision. This work is compared with previous implementations to measure performance.

Conclusion: The comparison analysis improves tumor segmentation and classification accuracy. The suggested method yields great outcomes.

Keywords: Brain Tumor; Adaptive Histogram Equalization; Pulse Coupled Neural Networks; Deep Convolutional Network; Local Binary Patterns.

1. Introduction

Brain tumor detection and classification is one of the biomedical system's complex tasks due to the tumor region's complex and unique characteristics. Various surgical techniques are available to perform brain tumor surgery once the tumor is confirmed and the region is located. Keyhole surgery enabled medical professionals to access internal organs without significantly opening the body. Magnetic resonance imaging, ultrasound, and CT scanning imaging replaced X-ray imaging by forcing medical professionals to consider the body's illusive third dimension [1]. To examine the outputs of medical imaging systems to achieve the most benefit and easily interpret patient symptoms, image processing techniques designed initially for evaluating remote sensing data may be updated. The brain controls everyday living and is a vital nervous system organ. The brain processes sensory impulses, makes choices, and sends information to the muscles. A collection of aberrant brain cells develops uncontrollably in BTs, one of the worst brain conditions. Primary and secondary metastatic BTs exist. Human brain cells cause non-cancerous primary brain tumors (BTs). Secondary metastatic tumors spread to the brain by blood flow from other organs [2].

Digital imaging techniques have revolutionized the field of photography, medical imaging, and many other areas of human endeavor. Digital imaging techniques allow us to capture, store, and manipulate images easily. They are more convenient than traditional imaging methods because they do not require film or darkroom equipment. Digital imaging techniques are faster than traditional methods. Digital imaging techniques produce high-quality images that are sharp, clear, and have a wide range of colors. By preprocessing, it is possible to enhance images, change the colors, adjust the contrast, and crop them to focus on specific details. Digital imaging techniques are often more cost-effective than traditional methods, requiring less equipment and consumables. They also allow for the reuse of imaging equipment, reducing the need for costly replacements. [3]. In addition, the World Health Organisation (WHO) categorized BTs into four groups (Grade I–IV) according to whether or not they cause cancer. Magnetic resonance imaging (MRI) and Computer Tomography (CT) are the two methods that are often used in the process of identifying and evaluating BTs [4]. Malignant BTs of grades III and IV develop rapidly, metastasize (spread to other regions of the body), and adversely influence healthy cells.

Brain tumors are caused by abnormally growing brain cells. Primary brain tumors begin in the brain, whereas secondary tumors begin in other bodily organs such as the colon, lung, or skin before spreading to the brain. According to the cells a tumor starts in, many types exist. Glioma, pituitary, and meningioma are the three primary varieties of tumors [5]. Women and older persons are more likely to develop meningiomas, which often result in low-grade malignancy. They usually go through three grades and develop slowly. Meningiomas develop in the three membrane-covered meninges that surround and safeguard the brain. One of the world's most deadly and aggressive diseases is a brain tumor, and early detection of these tumors is crucial for clinical evaluation and treatment planning [6].

Brain tumor pictures may often be obtained using MRI, a popular imaging method—different imaging modalities. T1, T1CE, T2, and FLAIR are different types of MRI sequences used to produce images of the brain. T1 (T1-weighted) MRI sequence provides detailed images of brain anatomy and is commonly used to evaluate brain structure. T1 images are useful for identifying structures with high fat or protein content, such as the myelin sheath surrounding nerve fibers. T1CE (T1-weighted contrast-enhanced) MRI sequence is similar to T1 but uses a contrast agent to enhance blood vessels' and tumors' visibility. T1CE images can detect tumors or other abnormalities difficult to see with other MRI sequences. T2 (T2-weighted) MRI sequence is sensitive to changes in water content, which makes it useful for detecting abnormalities in the brain, such as edema (swelling) and inflammation. T2 images are also helpful in identifying tumors, as they often have a higher water content than normal brain tissue. FLAIR (fluid-attenuated inversion recovery) MRI sequence is similar to T2 but uses a specialized technique to suppress the signal from Cerebrospinal Fluid (CSF) in the brain. FLAIR images are commonly used to detect lesions associated with Multiple Sclerosis (MS) and other neurological disorders [7].

Deep neural networks have been increasingly popular among academics in recent years due to their excellent performance and high picture segmentation accuracy. CNNs are a specific type of deep neural network that can identify and extract details from images. For automated brain tumor segmentation in MRI scans, many studies have employed CNN. This article aims to investigate the

architecture of the widely used segmentation CNN models (SegNets, U-Net, and Resnet18) and identify the benefits of each model to create hybrid designs that incorporate the benefits of the widely used CNN models. The hybrid design is anticipated to produce a more accurate outcome. [8]. Compared to 2D CNNs, 3D Convolutional Neural Networks (CNNs), one of the DL-based methods, are better suited for volumetric segmentation tasks [9]. In contrast, 2D-CNN takes fewer computing resources and training data and examines the existence of tumors in each slice in a 2D manner. However, 2D-CNNs cannot handle the 3D sequential data, which is essential for volumetric segmentation, and as a result, the segmentation performance is negatively impacted [10].

The images are preprocessed using normalization smoothing, linear filtering, and adaptive histograms using this work. To carry out the classification procedure, statistical and LBP characteristics are retrieved from the pictures that have been preprocessed. Image segmentation is accomplished with the help of a DCNN. The input pictures are classified as normal or having a tumor using PCNN.

The major contributions of this work is:

• The application of normalization, smoothing, linear filtering, and adaptive histogram equalization as preprocessing steps helps enhance the quality of the input images.

• These techniques can improve image contrast, reduce noise, and enhance important features, making subsequent analysis more effective.

• Statistical features can capture global image characteristics, while LBP can highlight local texture patterns. The combination of these techniques contributes to a richer feature set for subsequent classification.

The organization of this paper's structure is as follows: An overview of the deep learning idea and architecture is provided in Section II, the stages of the suggested technique are explained in Section III, the experimental results and analysis are shown in Section IV, and the conclusion and recommendations are provided in Section V.

1.1. Literature Survey

Previously, several techniques have been proposed to perform the brain tumor segmentation and classification process. The anomaly region should be located properly before classification in brain tumor detection. The feature of the anomaly region is further used for the classification. Machine learning is commonly utilized for tumor categorization into suitable classifications. Some previous techniques proposed for brain tumor detection and classification are discussed below.

Javaria *et al.* proposed the Weiner filter, and numerous wavelet bands are used to improve and denoise the input slices. Tumor pixel subgroups are identified using Potential Field (PF) clustering. Additionally, the tumor zone is segregated in FLAIR and T2 MRI utilizing a global threshold and several mathematical morphological approaches. For exact classification, Gabor Wavelet Transform (GWT) and Local Binary Pattern (LBP) characteristics are merged [11].

Tanzila *et al.* proposed that the novel method using a visual geometry group (VGG-19) is adjusted to learn the features, which are then integrated with manually constructed qualities using a serial-based technique. The grab-cut technique is used to divide the real lesion symptoms accurately. Classifiers are provided with a merged vector due to using entropy to optimize these properties for precise and speedy classification. Multimodal Brain Tumor Segmentation (BRATS) databases from 2015, 2016, and 2017 are among the best challenge databases for evaluating the proposed model [12].

Amin *et al.* proposed an automated approach to distinguish between brain MRI scans with cancer without malignancy. The segmentation of potential lesions has used a variety of methodologies. Then, considering form, texture, and intensity, a feature set is selected for each applicant lesion. The Support Vector Machine (SVM) classifier is then used for the collection of features to compare the proposed framework's precision using various cross-validations. Three test datasets, including the Harvard, RIDER, and Local benchmarks are used to validate the proposed technique [13].

Marcin *et al.* proposed a cutting-edge Convolutional Neural Network (CNN) and conventional architecture combined Correlation Learning Mechanism (CLM) for deep neural network methods. CNN uses a neural support network to

determine the best pooling and convolution layers files. As a result, the primary neural classifier gains efficiency and learns more quickly [14].

Mesut *et al.* proposed a brand-new Brain MRNet convolutional neural network model. This design contains a residual network based on attention modules and hypercolumn technology. First, Brain MRNet does picture preprocessing. Then, utilizing image augmentation methods for each picture, this process is conveyed to attention modules. Convolutional layers receive the picture after attention modules have chosen critical portions of the image. Hypercolumn is a key method the Brain MRNet model uses in its convolutional layers. The array structure in the final layer of the Brain MRNet model retains the characteristics taken from each layer using this method. The best and most valuable features are to be chosen among the features kept in the array. The BrainMRNet model was used to identify brain tumors using readily available magnetic resonance scans [15].

Ling *et al.* suggested a belief function-depend, semisupervised learning medical image segmentation network dubbed ELUNet. To create a lightweight Unet, we first updated the Unet foundation; then, for high-level semantic evidence combination and decision, moved the feature map from ELUnet to an ENN component. Arrive at a final segmentation result, Dempster's rule integrated the results from LUNet and ENN. Future research focuses on 3D volume segmentation and uncertain boundary analysis for medical imaging [16].

Guohua *et al.* proposed that each modality was exposed to a global hostile disturbance, and the effects on each modality and the overall MRI images were assessed. The efficacy of the four treatment approaches was compared individually. The findings show that: regardless of the amount of perturbation, accuracy performance is significantly affected by adversarial perturbation; performance differences when using multiple modalities are closely related to the intensity distribution [17].

The existing works are characterized by their high computational complexity and low accuracy. When just one modality is under assault, there is a considerable impact on the accuracy performance brought on by adversarial perturbation.

The motivation for the proposed method is:

1. To identify the presence of a tumor in the brain region from a brain tumor by analyzing the pixel characteristics using multiple significant features with recent classification techniques.

2. To improve the overall performance of the proposed method, brain tumor detection, and classification over different datasets.

2. Materials and Methods

2.1. Block Diagram

The detailed block concerning suggested PCNN segmentation and DCNN classification of brain tumors is shown in Figure 1. Here, picture preparation is carried out. Image normalization, smoothing, and adaptive histogram equalization are all parts of the preprocessing stage. Image normalization is done based on the minimum and maximum pixel values. The normalizing operation is carried out using the average value of the picture matrix. Following normalizing, linear smoothing is used to amplify the pictures. Additional feature extraction is done to extract other features, including statistical, texture, and PCNN features. PCNN is sometimes used for categorization, such as determining if something is normal or malignant.

2.2. Normalization

The dataset values range from positive to negative in all four columns. This study uses min-max normalization to limit the data to those between 0 and 1 [18-20]. Min-Max normalization preserves the characteristics' linear transformation. The equation represents the Minmax normalization. The property's minimum value is min_i, and its highest value is max_i (Equation 1).

$$N = \frac{n_i - min_i}{max_i - min_i} \qquad (1)$$

2.3. Smoothing by Linear Filter

The result value in the output image pixel $I_A(i, j)$ is calculated using linear operations as a linear combination of brightness near the input image pixel *I(i,j)*. For the sake of this approach, it presupposed that
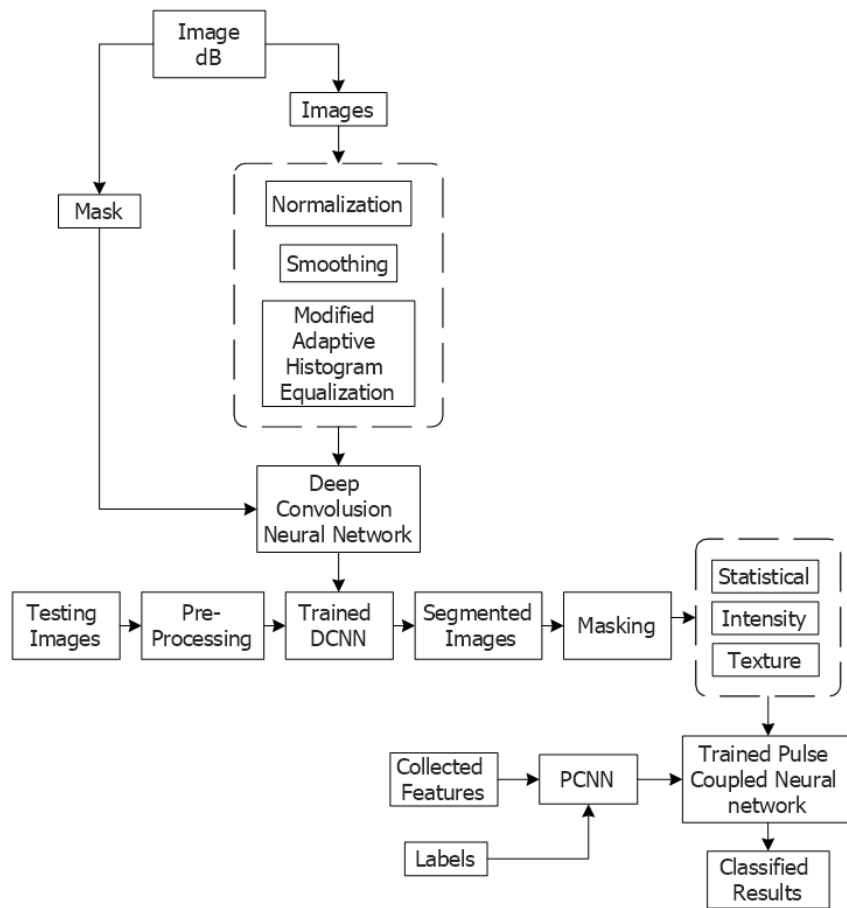
Figure1. Block diagram of the proposed method

I is an n, m image, and A is the convolution kernel or the filter mask of the linear filter, which is an mm mask [21-22]. The discrete convolution yields the filtered form of I, as shown below (Equation 2).

$$I_A(i,j) = I * A = \sum_{h=n/2}^{n/2} \sum_{k=m/2}^{m/2} A(h,k)I(i-h, j-k) \qquad (2)$$

$i = 1$ to n, and $j = 1$ to m. The value this filter replaces j with a weighted sum of i values in the vicinity of (i, j). The filter applies average smoothing if none of the items is negative. If none of the items in the signal is negative, this does not affect the ability of the filter to apply average smoothing. The filter still takes the average of the adjacent values, whether positive or negative. The output of the filter is the smoothed signal, which has fewer high-frequency components than the original signal. This can be useful for reducing noise or other unwanted features in the signal. Next, a matrix of the region of interest is created by subtracting the matrix of the aberrant brain scan picture from that of the typical brain image.

2.4. Adaptive Histogram Equalization

Contrast-constrained adaptive histogram equalization has shown successful results on medical images. This strategy's foundation divides the image into several equal-sized, non-overlapping sections. Produce an excellent statistical estimate for 512×512 images. The number of regions is frequently selected to be equal to 64 by equally dividing the image by 8 in each direction [23]. The divide results in three different groups of territories. One category with only four locations is the class of corner regions. The second group consists of 24 regions in the class of border areas. All areas of the image border outside the corners fall under this category. The last category, which comprises all 36 remaining regions, is called the class of inner regions. The histogram for each region is first calculated using this technique. The intended limit for contrast expansion is then used to define a clip limit for clipping histograms [24]. The resulting contrast-limited histograms' cumulative distribution functions, or CDF, are then computed for grayscale mapping.

2.5. DCNN

This work performs the classification using a pre-trained VGG-16 neural network model trained on more than one million annotated pictures from massive datasets like ImageNet. The average-pooling layer, sometimes called the Global Average Pooling Layer (GAP), reduces the whole amount of limits in the model to prevent overfitting. However, average pooling significantly reduces the spatial dimensions compared to max-pooling. This work performs the classification using a pre-trained VGG-16 neural network model trained on more than one million annotated pictures from massive datasets like ImageNet. For this study, the architecture has been modified [25]. As shown in the proposed model, the suggested design substitutes an average-pooling layer for the final max-pooling layer of a conventional VGG-16. By reducing the total number of parameters in the model, the average-pooling layer, the GAP, conducts spatial pooling of the feature map to prevent overfitting [26]. Comparatively, average pooling significantly reduces the spatial dimensions over max-pooling. Figure 2 depicts the DCNN architecture. Table 1 shows the Parameter Specification.

Table 1. Parameter Specification

Layer	Parameters
CONV 1	220
CONV 2	3820
POOL 1	0
CONV 3	7140
CONV 4	15440
POOL 2	0
CONV 5	14480
CONV 6	14480
FC 1	128164
FC 2	650

2.6. Statistical Features

Mean (M):

The average pixel intensity of an area may be found by finding its mean. A higher mean may indicate concentrated brilliant pixels in tiny areas [27] (Equation 3).

$$\bar{x} = \frac{1}{n}\left(\sum_{i=1}^{n} x_i\right) = \frac{x_1 + x_2 + \cdots + x_n}{n} \quad (3)$$

Arithmetic means of a set of numbers $x_1 + x_2 + \cdots + x_n$ is typically denoted by (x_i) and the intensity value of i-th pixel, n is the number of pixels in the image.

Standard Deviation (σ):

Measures the image's average contrast [28] (Equation 4).

$$\sigma = \sqrt{\frac{1}{N-1}\sum_{i=1}^{N}(x_i - \bar{x})^2} \quad (4)$$

x_i represents the intensity value of the i-th pixel, $\bar{x}$ is the mean value of these observations.

Third Moment (μ3):

Skewness is a metric of the data imbalance relative to the model mean [29] (Equation 5).

$$\tilde{\mu}_3 = \frac{\frac{1}{N}(\sigma)^2}{\sigma^2} \quad (5)$$

where σ is the standard deviation.

Entropy (e): The input image's texture may be described using entropy, a statistical measure of unpredictability [30] (Equation 6).

$$EN = -\sum_{i=1}^{N_G} p(x_i)\log(p(x_i)) \quad (6)$$

Where N_G is the number of intensity levels, and $p(x_i)$ is the normalized histogram value for intensity (x_i):

2.7. LBP

The Local Binary Pattern (LBP) links the study of occurrences and the analysis of local structures. Each image pixel is represented by the LBP technique using a binary pattern [31]. The latter is based on the variance between the grey pixel level value and its radially centered, circular neighborhood with a radius R provided. The LBP codes are therefore calculated as (Equation 7)

$$LBP_{P,R(qc)} = \sum_{P=0}^{P-1} s(x)\ 2^p \qquad (7)$$

The differential in brightness between the central pixel (qc) and the neighboring pixels (qp) within the circle with radius R and P is represented by the expression $x = qp.qc$. Furthermore, $s(x)$ is (Equation 8):

$$S(x) = \begin{Bmatrix} 1 & x \geq 0 \\ 0 & otherwise \end{Bmatrix} \qquad (8)$$

The pixels in the area are organized in a circle. The estimation method is therefore utilized for neighbors that are not exactly in the middle of pixels. The parity bit, produced by arranging every bit clockwise or anticlockwise, is then communicated to the central pixel. Since each number is 0 or 1, the LBP codes vary from 0 to 1. Because of the sign function s, the LBP code is constant against any monotonic variation in image brightness (x). The texture may then be described using the histogram of each of these labels [32]. Thus, an LBP histogram vector h may represent a picture, and the dispersion of LBP patterns can be used to characterize a texture image (Equation 9).

$$h = \sum_{i=1}^{W} \sum_{j=1}^{H} \times ((i,j) - k) \qquad (9)$$

2.8. Pulse Coupled Neural Network (PCNN)

PCNN is a type of neural network inspired by the functioning of biological neurons and their behavior in response to external stimuli. The main motivation behind using PCNN is its ability to process images and other types of signals similar to how the human brain processes information. PCNNs differ from other neural networks in several ways. First, PCNNs use a different activation function than other types of neural networks. Rather than using a traditional sigmoid or ReLU function, PCNNs use a pulse function based on biological neurons' behavior. Second, PCNNs are designed to process signals in a way that is similar to the way that biological neurons process information. This allows them to detect patterns and features in signals that might be difficult to detect using other types of neural networks. Another key difference between PCNNs and other types of neural networks is how they process information over time. Overall, the motivation behind using PCNN is to create a neural network

architecture better suited for processing signals in a way similar to how the human brain processes information.

The PCNN-founded procedures are effectively applied in image applications of interpretation. Elkhorn's cortical neuron model was modified to create the Pulse Coupled Neuron (PCN) model utilized in PCNN. Feature extraction, picture segmentation, and image smoothing may be done with pulse-linked neural networks [33]. The Feeding and Linking compartments are the primary compartments in a PCNN neuron. Each interacts with nearby neurons through the synaptic weights M and W. All keep their original states, albeit with a decay factor. The input stimulus, S, is only received by the feeding segment. These two compartments' values are decided by (Equations 10, 11),

$$F_{ij}[n] = e^{\alpha_L \delta_n} F_{ij}[n-1] + S_{ij} + V_F \sum_{kl} M_{ijkl} Y_{kl}[n-1] \qquad (10)$$

$$L_{ij}[n] = e^{\alpha_L \delta_n} L_{ij}[n-1] + V_L \sum_{kl} W_{ijkl} Y_{kl}[n-1] \qquad (11)$$

Where F_{ij} is the (i, j) neuron's input region and L_{ij} is the consistent Connecting section. Y_{kl} The neuronal outputs from an earlier iteration [n−1]. The memory of the initial state exists in both compartments and degrades with time by the exponential term. V_F and V_L are normalizing constants. These variables are employed to adjust the resulting correlation to avoid saturating.

The connection strength β regulates the combination. Calculating the internal activity is done using (Equations 12, 13),

$$U_{ij}[n] = F_{ij}[n][1 + \beta L_{ij}[n] \qquad (12)$$

$$Y = \begin{Bmatrix} 1\ if\ U_{ij}[n] > \theta_{ij}[n] \\ 0 \qquad otherwise \end{Bmatrix} \qquad (13)$$

The threshold is dynamic because it dramatically increases in value when the neuron fires ($Y > $). When the neuron fires again, this value starts to decline. The method is explained by (Equation 14),

$$\theta_{ij}[n] = e^{\alpha_L \delta_n} \theta_{ij}[n-1] + V_\theta Y_{ij}[n] \qquad (14)$$

$V\theta$ is a significant variable typically more than an order of magnitude larger than the overall average of U. Table 2 Shows the Specification of the PCNN network.

Table 2. PCNN Specification

Layer	Feature map size
Convolution	24X24
Max pooling	12X12
Dropout layer	12X12
Convolution	10X10
Output layer	2X2

3. Results

A computer system with Windows 10 ZV and a Geforce RTX 2080 Ti GPU was employed during the experiment. The DCNN model was tested using Python in the Keras module on an Intel Xeon-2620 with a Core i5-2.4GHz CPU and 16 GB of RAM.

3.1. Dataset

In this work, we used the BRATS 2020 dataset. The collection includes 293 High-Grade Glioma (HGG) and 76 Low-Grade Glioma (LGG) pre-operative images in T1, T2, T1ce, and FLAIR MRI modalities. Experienced neuroradiologists approved the annotations. The anatomical template of the T1 picture from the same scan is co-registered with the same scan's T2, T1ce, and FLAIR images. All the pictures have been stripped of their skulls and interpolated to the exact resolution (1mm×1mm×1mm). For 237 HGG images, OS's features and resection status are presented individually. With the same preprocessing, the validation and test datasets consist of 125 and 166 MRI images [34]. The dataset comprises all sets' training set survival days, age, and resection status. Figure 2. shows the sample images from the dataset. Table 3 shows the clinical information of participants for BRATS 2020 dataset.
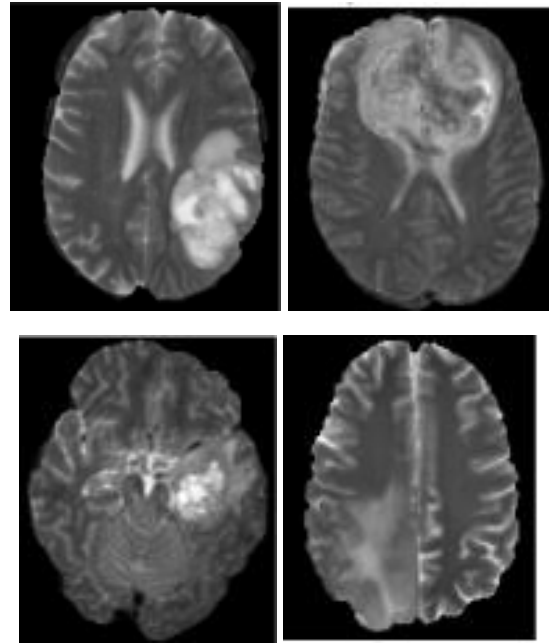
3.2. Evaluation Metric

Accuracy

Accuracy is used to calculate the rate of correctly classifying tumors (Equation 15).

$$Accuracy = \frac{(TP + TN)}{(TP + TN) + (FP + FN)} \times 100 \quad (15)$$

Sensitivity

Figure 2. Sample images from the dataset

Table 3. Clinical information of participants for BRATS 2020 dataset

Participants ID	Age	Grnder	Sex
001	45	Male	M
002	38	Female	F
003	50	Male	M
004	32	Female	F
005	25	Male	M

Sensitivity determines a technique's sensitivity and computes the tumor detection rate [35-36] (Equation 16).

$$Sensitivity = \frac{(TP)}{(TP + FN)} \times 100 \quad (16)$$

Specificity

The ratio of true negatives to true positives is specificity [37-38] (Equation 17).

$$Specificity = \frac{(TN)}{(TN + FP)} \times 100 \quad (17)$$

Precision

Precision describes the number of digits used to express a value [39] (Equation 18).

$$Precision = \frac{(TP)}{(TP + FP)} \times 100 \quad (18)$$

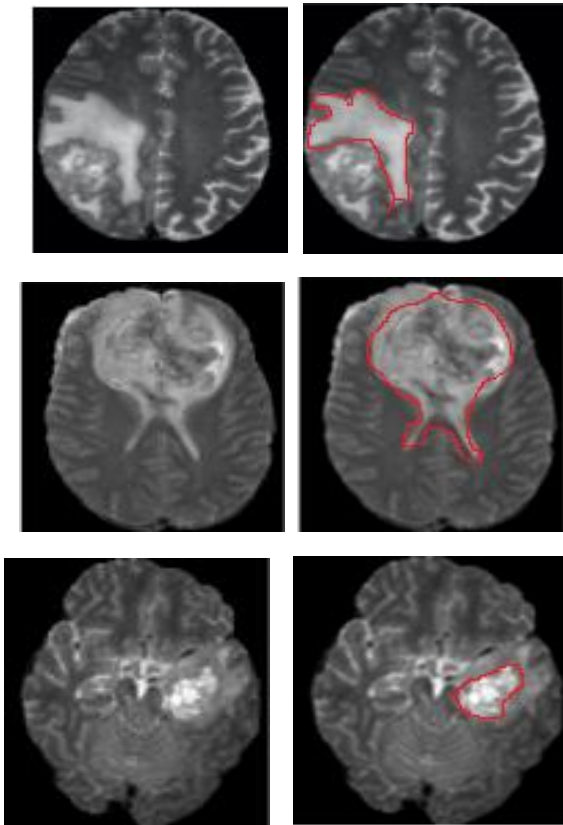TP – True Positives, TN - True Negatives, FP- False Positives, FN- False Negatives.

Figure 3. Segmented images from sample images

4. Discussion

Table 4 shows the performance of the proposed method based on Training and testing validation. The 50 percentage and 50 percentage of testing images achieve 94.18 of accuracy. The 60 percentage and 40 percentage of testing images achieve 91.13 of accuracy. The 70 percentage and 30 percentage of testing images achieve 99.35 of accuracy.

Table 5 shows the comparative performance of the proposed method. The existing DNN [1] method has 98.5 of accuracy, 95.89 of sensitivity, 96 of specificity, and 99.54 of precision. LU-NET [12] achieves 98% of accuracy, 95% of specificity, and 97% of precision. The existing DNN [13] method has 99.12% of accuracy and 100% of sensitivity. This work got 99.35 in accuracy, 99.78 in sensitivity, 98.45 in specificity, and 99.61 in precision.

Figure 3 Sample images from the dataset. Figure 4 shows the comparative performance of accuracy. Figure 5 shows the comparative performance of precision. Figure 6 shows the training accuracy of the proposed method.

5. Conclusion

The application of the suggested model demonstrates that the segmentation preprocessing step can be skipped when using PCNNs, and the PCNN image signature offers a significant discriminant feature for classification. The proposed model is tested using a dataset that has never been seen before to ensure that the model does not succumb to the overfitting issue caused by a small dataset size. It is possible to employ PCNN and DCNN merging as complementary feature extractors for pictures. This study classified brain tumor pictures using DCNN pre-trained models with PCNNs. The BRATS 2020 dataset was used to train and test the model, which yielded a 99.35% of accuracy rate.
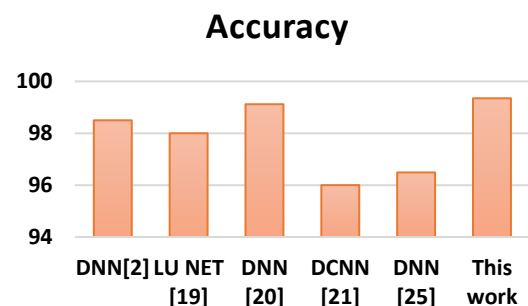

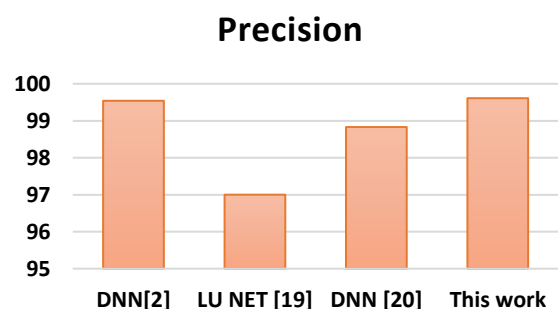
Figure 4. Comparative performance of accuracy

Figure 5. Comparative performance of precision

Table 4. Performance of proposed method based on training and testing validation

Training	Testing	Accuracy
40	60	65.17
50	50	72.36
60	40	84.18
70	30	91.13
80	20	99.35

Table 5. Comparative performance of the proposed method

Method	Accuracy	Sensitivity	Specificity	Precision
DNN [2]	98.5	95.89	96	99.54
LU NET [19]	98	-	95	97
DNN [20]	99.12	100	96.42	98.83
DCNN [21]	96.0	100	-	-
DNN [20]	96.49	98.5	98.9	-
This work	99.35	99.78	98.45	99.61
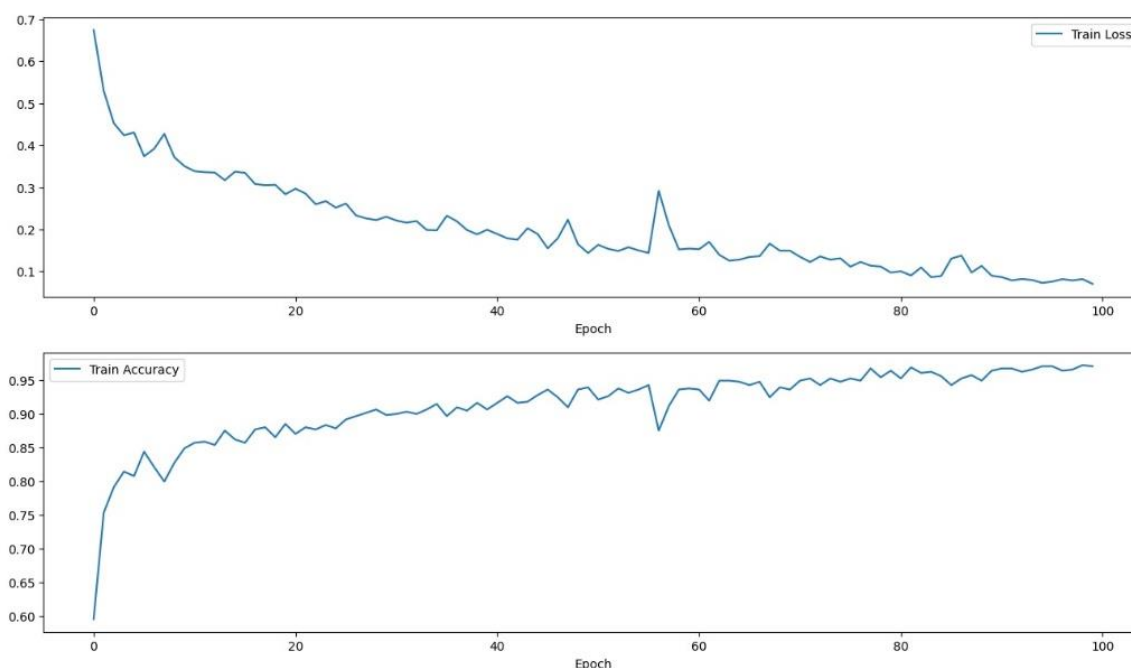
Figure 6. Training accuracy of the proposed method

Acknowledgment

References

1- Raza, Asaf, Huma Ayub, Javed Ali Khan, Ijaz Ahmad, Ahmed S. Salama, Yousef Ibrahim Daradkeh, Danish Javeed, Ateeq Ur Rehman, and Habib Hamam. "A hybrid deep learning-based approach for brain tumor classification." *Electronics* 11, no.7: 1146, (2022).

2- Woźniak M, Siłka J, Wieczorek M. Deep neural network correlation learning mechanism for CT brain tumor detection. *Neural Computing and Applications*; 16:1-6, (2021).

3- Sobhaninia, Z., Rezaei, S., Karimi, N., Emami, A., & Samavi, S. Brain tumor segmentation by cascaded deep neural networks using multiple image scales. In *2020 28th Iranian Conference on Electrical Engineering (ICEE)* (pp. 1-4). IEEE, (2020, August).

4- Kumar, Sharan, and Dattatreya P. Mankame. "Optimization driven deep convolution neural network for brain tumor classification." *Biocybernetics and Biomedical Engineering* 40, no. 3: 1190-1204, (2020).

5- Zhou, T., Canu, S., Vera, P., & Ruan, S. Brain tumor segmentation with missing modalities via latent multi-source correlation representation. In *International Conference on Medical Image Computing and Computer-Assisted Intervention* (pp. 533-541). Springer, Cham, (2020, October).

6- Nayak, Dillip Ranjan, Neelamadhab Padhy, Pradeep Kumar Mallick, Mikhail Zymbler, and Sachin Kumar. "Brain tumor classification using dense efficient-net." *Axioms* 11, no. 1: 34, (2022).

7- Abd El Kader, Isselmou, Guizhi Xu, Zhang Shuai, Sani Saminu, Imran Javaid, and Isah Salim Ahmad. "Differential deep convolutional neural network model

for brain tumor classification." *Brain Sciences* 11, no. 3: 352, (2021).

8-Ayadi, Wadhah, Imen Charfi, Wajdi Elhamzi, and Mohamed Atri. "Brain tumor classification based on hybrid approach." *The Visual Computer* 38, no. 1 (2022): 107-117.

9- Ullah, Z., Usman, M., Jeon, M., & Gwak, J. (2022). Cascade multiscale residual attention cnns with adaptive roi for automatic brain tumor segmentation. *Information Sciences*, *608*, 1541-1556.

10- Sharif, M. I., Li, J. P., Khan, M. A., & Saleem, M. A. (2020). Active deep neural network features selection for segmentation and recognition of brain tumors using MRI images. *Pattern Recognition Letters*, *129*, 181-189.

11- Amin, J., Sharif, M., Raza, M., Saba, T., & Anjum, M. A. (2019). Brain tumor detection using statistical and machine learning method. *Computer Methods and Programs in Biomedicine*, *177*, 69-79.

12- Saba, T., Mohamed, A. S., El-Affendi, M., Amin, J., & Sharif, M. (2020). Brain tumor detection using fusion of hand crafted and deep learning features. *Cognitive Systems Research*, *59*, 221-230.

13- Amin, J., Sharif, M., Yasmin, M., & Fernandes, S. L. (2020). A distinctive approach in brain tumor detection and classification using MRI. *Pattern Recognition Letters*, *139*, 118-127.

14- Woźniak M, Siłka J, Wieczorek M. Deep neural network correlation learning mechanism for CT brain tumor detection. *Neural Computing and Applications*. 2021; 16:1-6.

15- Toğaçar, M., Ergen, B., & Cömert, Z. (2020). BrainMRNet: Brain tumor detection using magnetic resonance images with a novel convolutional neural network model. *Medical Hypotheses*, *134*, 109531.

16- Huang L, Ruan S, Denoeux T. 2021. Belief function-based semi-supervised learning for brain tumor segmentation. In2021 IEEE 18th International Symposium on Biomedical Imaging (ISBI) 2021 Apr 13 (pp. 160-164). IEEE.

17- Cheng G, Ji H. Adversarial perturbation on MRI modalities in brain tumor segmentation. IEEE Access. 2020 Oct 12; 8:206009-15.

18- Abd El Kader, I., Xu, G., Shuai, Z., Saminu, S., Javaid, I., & Salim Ahmad, I. (2021). Differential deep convolutional neural network model for brain tumor classification. *Brain Sciences*, *11*(3), 352.

19- Rai, H. M., & Chatterjee, K. (2020). Detection of brain abnormality by a novel Lu-Net deep neural CNN model from MR images. *Machine Learning with Applications*, *2*, 100004.

20- Siar, M., & Teshnehlab, M. (2019, October). Brain tumor detection using deep neural network and machine learning algorithm. In *2019 9th international conference on computer and knowledge engineering (ICCKE)* (pp. 363-368). IEEE.

21- Subashini, M. M., & Sahoo, S. K. Brain tumor detection using Pulse coupled neural network (PCNN) and back propagation network, (2012).

22- Ullah Z, Usman M, Jeon M, Gwak J. Cascade multiscale residual attention cnns with adaptive roi for automatic brain tumor segmentation. *Information Sciences*; 1;608:1541-56, (2022)

23- Ramamoorthy, M., Qamar, S., Manikandan, R., Jhanjhi, N. Z., Masud, M., & AlZain, M. A. Earlier detection of brain tumor by preprocessing based on histogram equalization with neural network. In *Healthcare* (Vol. 10, No. 7, p. 1218). MDPI, (2022, June).

24- Kabir, M. A. Automatic brain tumor detection and feature extraction from mriimage. GSJ, 8(4), (2020).

25- Zeineldin RA, Karar ME, Elshaer Z, Wirtz CR, Burgert O, Mathis-Ullrich F. Explainability of deep neural networks for MRI analysis of brain tumors. *International Journal of Computer Assisted Radiology and Surgery.*; 23:1-1, (2022).

26- Kapoor, A., & Agarwal, R. Brain Image Segmentation based on U-Net Architecture with Adaptive Histogram Equalization. In *2021 9th International Conference on Reliability, Infocom Technologies and Optimization (Trends and Future Directions) (ICRITO)* (pp. 1-5). IEEE, (2021, September).

27- Amin, J., Sharif, M., Yasmin, M., & Fernandes, S. L. Big data analysis for brain tumor detection: Deep convolutional neural networks. *Future Generation Computer Systems*, *87*, 290-297, (2018).

28- Deepak, S., & Ameer, P. M. Brain tumor classification using deep CNN features via transfer learning. *Computers in Biology and Medicine*, *111*, 103345, (2019).

29- Irmak, E. Multi-classification of brain tumor MRI images using deep convolutional neural network with fully optimized framework. *Iranian Journal of Science and Technology, Transactions of Electrical Engineering*, *45*(3), 1015-1036, (2021).

30- Tang, Chaosheng, Bin Li, Junding Sun, Shui-Hua Wang, and Yu-Dong Zhang. "GAM-SpCaNet: gradient awareness minimization-based spinal convolution attention network for brain tumor classification." *Journal of King Saud University-Computer and Information Sciences*, (2023).

31- Ismael, M. R., & Abdel-Qader, I. Brain tumor classification via statistical features and back-propagation neural network. In 2018 IEEE international conference on electro/information technology (EIT) (pp. 0252-0257). *IEEE,* (2018, May).

32- Kaplan, K., Kaya, Y., Kuncan, M., & Ertunç, H. M. Brain tumor classification using modified local binary patterns (LBP) feature extraction methods. *Medical Hypotheses*, 139, 109696, (2020).

33- Henry T, Carré A, Lerousseau M, Estienne T, Robert C, Paragios N, Deutsch E. Brain tumor segmentation with self-ensembled, deeply-supervised 3D U-net neural networks: a BraTS 2020 challenge solution. *In International MICCAI Brainlesion Workshop 2020 Oct 4. Springer, Cham*, (pp. 327-339), (2020).

34- Henry, Theophraste, Alexandre Carré, Marvin Lerousseau, Théo Estienne, Charlotte Robert, Nikos Paragios, and Eric Deutsch. "Brain tumor segmentation with self-ensembled, deeply-supervised 3D U-net neural networks: a BraTS 2020 challenge solution." In Brainlesion: Glioma, Multiple Sclerosis, Stroke and Traumatic Brain Injuries: 6th International Workshop, BrainLes 2020, Held in Conjunction with MICCAI 2020, Lima, Peru, October 4, Revised Selected Papers, Part I 6, pp. 327-339. *Springer International Publishing, 2021,* (2020).

35- Dehyadegari, L., & Khajehasani, S. Magnetic Resonance Imaging Image Segmentation and Brain Tumor Detection Using Pulse-Coupled Neural Networks. *Journal of Engineering Science*, *17*(1), 1-16, (2021).

36- Niepceron, B., Grassia, F., & Moh, A. N. S. Brain Tumor Detection Using Selective Search and Pulse-Coupled Neural Network Feature Extraction. *Computing and Informatics*, *41*(1), 253-270, (2022).

37- Shanker, R., & Bhattacharya, M. Classification of brain MR images using Modified version of Simplified Pulse-Coupled Neural Network and Linear Programming Twin Support Vector Machines. *The Journal of Supercomputing*, 1-33, (2022).

38- Li, M., Kuang, L., Xu, S., & Sha, Z. Brain tumor detection based on multimodal information fusion and convolutional neural network. *IEEE Access*, *7*, 180134-180146, (2019).

39- Xiao, F., Lv, S., Zong, Z., Wu, L., Tang, X., Kuang, W., & Guo, H. Cerebrospinal fluid biomarkers for brain tumor detection: clinical roles and current progress. *American Journal of Translational Research*, *12*(4), 1379, (2020).